Geophysical Research Letters

RESEARCH LETTER
10.1029/2023GL102782

The Energetic 2022 Seismic Unrest Related to Magma Intrusion at the North Mid-Atlantic Ridge

S. Cesca[1], M. Metz[1,2], P. Büyükakpınar[1,2], and T. Dahm[1,2]

[1]GFZ German Research Centre for Geosciences Potsdam, Potsdam, Germany, [2]University of Potsdam, Potsdam, Germany

Key Points:

- Analysis of a short, intense seismic swarm at the Mid-Atlantic Ridge
- Identification of unusual, thrust focal mechanisms in an extensional environment
- Swarm triggered by dike intrusion at the mid-ocean ridge

Supporting Information:

Supporting Information may be found in the online version of this article.

Correspondence to:

S. Cesca,
simone.cesca@gfz-potsdam.de

Citation:

Cesca, S., Metz, M., Büyükakpınar, P., & Dahm, T. (2023). The energetic 2022 seismic unrest related to magma intrusion at the North Mid-Atlantic Ridge. *Geophysical Research Letters*, *50*, e2023GL102782. https://doi.org/10.1029/2023GL102782

Received 27 JAN 2023
Accepted 23 JUN 2023

Author Contributions:

Conceptualization: S. Cesca, T. Dahm
Data curation: S. Cesca, M. Metz, P. Büyükakpınar
Formal analysis: S. Cesca, M. Metz, P. Büyükakpınar
Investigation: S. Cesca
Methodology: S. Cesca, M. Metz
Supervision: S. Cesca
Validation: S. Cesca
Visualization: S. Cesca, M. Metz, P. Büyükakpınar
Writing – original draft: S. Cesca
Writing – review & editing: S. Cesca, M. Metz, P. Büyükakpınar, T. Dahm

Abstract A seismic swarm affected the 53.3°–54.3° Latitude North section of the Mid-Atlantic Ridge from 26 September to 10 December 2022. We rely on regional, teleseismic and array data to relocate 61 hypocenters and derive 77 moment tensors. The 2022 swarm released a cumulative moment equivalent to Mw 6.3. Seismicity was shallow (7 ± 3 km depth). Most earthquakes are located along the ridge axis with typical, NS oriented normal faulting mechanisms, but a few among the largest and latest earthquakes have unusual thrust mechanisms and locations as far as ∼25 km from the ridge. We attribute the swarm to a shallow magmatic intrusion, with a vertical dike first propagating ∼60 km along axis, accompanied by shallow normal faulting, and then thickening and triggering thrust earthquakes off the ridge, in response to compressive stress buildup. The unrest provides a rare example of an energetic, magmatic driven swarm episode at the mid-ocean ridge.

Plain Language Summary The largest plate boundary systems on Earth are Mid-ocean ridges (MOR), where the plates continuously drift apart and new lithosphere is constantly being formed. Although the process is well understood, we rarely detect spreading events at MOR, mainly because these regions are remote and local monitoring is rarely possible. In September–November 2022 a large, unusual seismic swarm occurred along a spreading center ridge segment of the North Mid-Atlantic Ridge. Despite the remoteness of the region, we managed to model regional and teleseismic data to perform earthquake relocation, depth estimation and moment tensor inversion. In this way, we could reconstruct the geometry and the evolution of the seismicity. We found that in the early days of the swarm, seismicity migrated unilaterally over ∼60 km along the ridge axis, from North to South, triggering normal faulting earthquakes, which are typical at MOR. Later, large thrust mechanisms, anomalous in an extensional environment, appeared and quickly became predominant. We explain seismological observations by a magmatic intrusion, which first propagated southward, producing shallow normal faulting earthquakes above the vertical magma dike, and later thickened, increasing compressional stresses on its sides, and triggering large thrust earthquakes.

1. Introduction

Mid-ocean ridges (MOR) are formed by the separation and spreading of divergent tectonic plates, accompanied by mantle upwelling and the formation of new oceanic lithosphere. Seismicity at MORs is generally confined within a narrow band with a few tens of kilometers width (Searle, 2013). Spatial distribution and focal mechanisms reflect the ridge segmentation, with normal faulting earthquakes along spreading center segments and strike-slips along transform faults (Rundquist & Sobolev, 2002); focal mechanisms for globally observed earthquakes are consistent with the tectonic stresses due to the plate kinematics (Isacks et al., 1968; Searle, 2013; Sykes, 1967; Weidner & Aki, 1973). Smaller earthquakes ($M < 3$) display a larger variety of mechanisms (Meier et al., 2021), including thrust components (Parnell-Turner et al., 2017).

Dike intrusions at MOR represent a fundamental process in the formation of new oceanic crust (Dziak et al., 2006), which is often accompanied by swarm-like seismicity (Ágústsdóttir et al., 2016, 2019; Keir et al., 2009; Sigmundsson et al., 2015; Wright et al., 2012). Swarms are seismic sequences lasting days to months (Benoit & McNutt, 1996; Chen & Shearer, 2011; Hill, 1977; Llenos & Van der Elst, 2019), with clustered spatial locations and most moment release occurring delayed after the swarm onset (Chen & Shearer, 2011; Passarelli, Rivalta, et al., 2018; Roland & McGuire, 2009). Earthquake swarms are observed at divergent plate boundaries, including along MORs (Bergman & Solomon, 1990; Dziak et al., 1995; Ruch et al., 2021; Sykes, 1970). Magmatic driven swarms at MORs are rarely reported or studied, mostly because of detection challenges at their remote locations (Dziak et al., 2006). It is often debated whether swarms in extensional domains are controlled

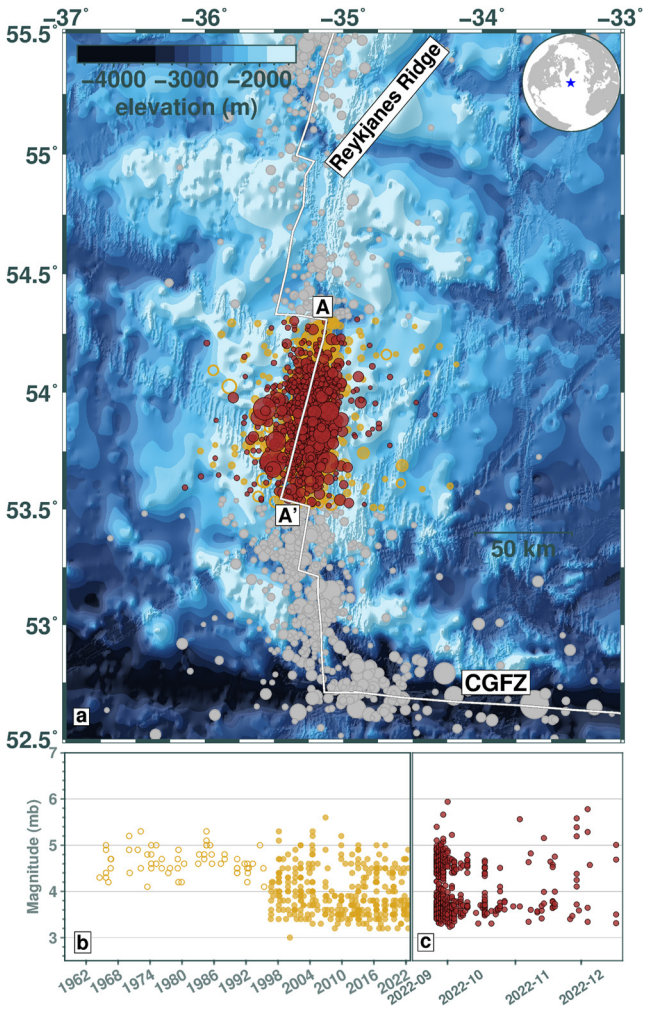

Figure 1. (a) Seismicity distribution at the swarm region, Mid-Atlantic-Ridge (see star location in the top right inset). Yellow circles indicate seismicity between 1958 and 2022, red circles swarm seismicity since mid August 2022. The seismic catalog is taken from the International Seismological Center, and bathymetry from Global Multi-Resolution Topography (Ryan et al., 2009), with white lines showing the plate boundaries (Bird, 2003). (b, c) Temporal evolution of the seismicity (b) before and (c) during the swarm episode, reporting average seismicity rates.

by magmatism or tectonics (Bergman & Solomon, 1990; Ruch et al., 2021; Schlindwein, 2012). An early recompilation of swarms at the Mid-Atlantic Ridge suggested that most of them could be explained by tectonic extensional stresses, but did not rule out a magmatic origin (Bergman & Solomon, 1990). Most of those swarms, however, neither affected large regions, not exceeding 20 km along the ridge and 15 km across it, nor displayed a clear migration, which is common for magmatic intrusions (e.g., Ágústsdóttir et al., 2016; Cesca et al., 2020; Dziak et al., 1995; Passarelli, Heryandoko, et al., 2018; Rivalta et al., 2015). Conversely, the analysis of later swarm episodes in extensional tectonic domains rather suggested magma dike intrusions as the driver (Dziak et al., 2006, 2007, 2012; Ruch et al., 2021; Schlindwein, 2012).

Local magma intrusions at the Mid-Atlantic Ridge have been hypothesized based on seismicity, hydroacoustic, and biological observations (Dziak et al., 2006; Giusti et al., 2018; Goslin et al., 2012; Simao et al., 2010), but with considerably lower magnitudes (Goslin et al., 2012; Simao et al., 2010). Magma-driven swarms have also been inferred at other MORs (Dziak et al., 2006, 2007, 2012; C. Müller & Jokat, 2000; Radha Krishna & Arora, 1998; Tolstoy et al., 2001), but also rarely reaching high magnitudes. Swarms with a comparable moment are reported at the Gakkel Ridge (C. Müller & Jokat, 2000; Tolstoy et al., 2001), during diking episodes at the East African Rift (Wauthier et al., 2016) and adjacent to the 2021 Fagradalsfjall dike intrusion, Iceland (Sigmundsson et al., 2022).

Earthquake swarms at ultraslow spreading ridges were found to occur at centers of magmatism, initiated by magma intrusions (Schlindwein, 2012). Similarly, many seismic swarms in the Afar triangle, along the Red Sea and Gulf of Aden ridges and the Afar rift, have been associated with rifting, intrusive episodes, sometimes leading to submarine volcanic eruptions (e.g., Ruch et al., 2021). Magmatic intrusions have also triggered large swarms in extensional tectonic domains, as for the 2022 Bransfield Strait, Antarctica, swarm, with ~85,000 earthquakes (Cesca et al., 2022).

The following arguments have been previously used to support the magmatic origin of seismicity at slow spreading ridges and divergent plate boundaries: seismicity at volcanic centers and/or at segments with large magmatic accretion, swarm-like seismicity patterns (Schlindwein, 2012; Shuler & Nettles, 2012), repeated swarm episodes in the same region (Schlindwein, 2012), seismicity migration (Bergman & Solomon, 1990; Rundquist & Sobolev, 2002; Shuler & Nettles, 2012), seismicity elongated along the ridge axis (Bergman & Solomon, 1990), clustered normal faulting earthquakes (Shuler & Nettles, 2012), and seafloor or geodetic evidence for volcanic vents and/or magma flows (Ruch et al., 2021). The type and geometry of focal mechanisms can also be used to discuss the origin of seismicity. Normal faulting focal mechanisms are both favored by magmatic or tectonic drivers (Cesca et al., 2022; Passarelli et al., 2015; Passarelli, Rivalta, et al., 2018). Strike-slip mechanisms with rupture planes oblique to the ridge axis, instead, can be triggered at the tip of migrating dikes and provide evidence for a magmatic driver (Hill, 1977; Passarelli et al., 2015). Finally, thrust mechanisms have been rarely reported in extensional domains (Ruch et al., 2021; Wolfe et al., 2012) and require a strong perturbation of the background, tectonic stress.

According to global catalogs, the seismic swarm (Figure 1) started on 26 September 2022, with a sharp seismicity increase, continuing with lower rates until early December 2022 (Figure 1c). The largest earthquakes occurred days after the unrest onset, confirming swarm-like seismicity. The seismicity is shallow and clustering along a slow spreading segment of the North Mid-Atlantic Ridge, at the Southern end of the Reykjanes Ridge and North of the Charlie-Gibbs Fracture Zone (Figure 1a). The spreading rate in the region is 95–125 mm/yr (Le Pichon, 1968; R. D. Müller et al., 2008). The global catalog in this region (Figure 1b) is more complete since

1996. The local background seismicity in the time period 1996–2022 (mb > 3.5) is ~12.6 evs/yr, with a cumulative moment release per year and km rift axis of ~2.9 10^{18} Nm/ykm, and a peak magnitude Mw 5.6 (International Seismological Centre, 2022). The 2022 swarm (Figure 1c) is outstanding both in terms of its rate (~3,024 evs/yr), moment release (~8.5·10^{21} Nm/ykm) and maximum magnitude (Mw 5.9).

Here we rely on seismic data at regional (500–1,000 km) to teleseismic distances (here up to 2,500 km), including the NOA seismic array, Norway (Norsar, 1971), to relocate the seismicity and infer moment tensors with a good azimuthal coverage (Figure S1 in Supporting Information S1). This helps to assess the spatiotemporal evolution of seismicity, track the magma dike migration and unravel seismogenic processes at the MOR.

2. Materials and Methods

2.1. Template Matching

Template matching helps the detection of weak earthquakes with similar locations and focal mechanisms as the templates (Gibbons & Ringdal, 2006; Peng & Zhao, 2009). Here template matching is used to identify the unrest onset. We rely on vertical raw signals recorded at the NORSAR arrays NOA (Figure S1 in Supporting Information S1) (Norsar, 1971), with high Signal-to-Noise ratios (Bungum et al., 1971). We process continuous data between 15 August and 15 December 2022. Records were visually inspected: noisy records of stations NBO00, NBO02, and NC205 were removed and swapped polarities corrected for (NAO05 and NB203). Raw velocity records were filtered in the frequency band 0.01–0.05 Hz, traces of different stations aligned based on the maximum correlation coefficient (CC) coefficient of the largest earthquake and stacked thereafter. Thereby uncorrelated noise was further reduced. We used two template events, representing the two prevailing types of focal mechanisms by their strongest events: the 26 September 2022, 09:59:57 UTC normal faulting and the 29 September 2022, 15:32:32 UTC thrust earthquake. Full template waveforms were extracted for a time window of 866 s, starting 100 s before the P phase and ending 500 s after the S phase (Figures S2 and S3 in Supporting Information S1). The waveform similarity was retrieved from the normalized cross CC (Gibbons & Ringdal, 2006). The CC is derived as the sum of signal amplitudes within a gliding window with the same length as the template waveform. The normalization is performed using the square root of the summed squared amplitudes of the template and the signal waveform. The detection threshold was set to a CC coefficient of 0.6, giving 174 earthquake detections with magnitudes down to 4.2. A lower CC of 0.5 resulted in an increased number of detections outside the study area. Results for different CC thresholds are illustrated in Figure S4 in Supporting Information S1.

2.2. Moment Tensor Inversion and Classification

Full and deviatoric moment tensor inversions are performed using Grond (Heimann et al., 2018), for 81 events exceeding Mw 4.5, providing robust solutions for a subset of 77 earthquakes (Data Sets S2 and S3). Figures S5 and S6 in Supporting Information S1 provide examples of waveform fits and moment tensor inversion results. Since both results using the two moment tensor constraints are similar, in terms of magnitude, depth, and geometry of the double couple components, we only discuss full moment tensor solutions. We fit full waveform displacement (vertical and transversal components) from broadband seismic stations located at less than 2,500 km epicentral distance (Figure S1 in Supporting Information S1). Synthetic seismograms are computed assuming a global mantle model with an average oceanic crust (Cesca et al., 2021). A bandpass in the range 0.015–0.040 Hz is applied to data and synthetics; the fit is estimated using an L1-norm. All seismic traces have been visually inspected, and a few traces removed in presence of noise or gaps. We set up Grond to perform 60,000 iterations. We assume an impulsive source time function and invert for the following parameters: centroid time, location and depth and 6 MT components. We repeat the inversion using all data, to obtain a so-called "best" solution, and for 100 bootstrap chains, where data are weighted differently, in order to estimate a "mean" solution and source parameter uncertainties. The resulting MT catalog (full MT mean solutions, Figure S7 in Supporting Information S1) was classified using Seiscloud (Cesca, 2020), with the Kagan angle (Kagan, 1991, 1992) as metric for the MT similarity (Figure S8 in Supporting Information S1). Seiscloud implements DBSCAN (Ester et al., 1996), a density based clustering algorithm, and its result depends on two parameters (N_{min}, ε). We choose $N_{min} = 3$ and $\varepsilon = 0.2$ (i.e., forming a cluster whenever for one earthquake there at least 3 other neighboring events with a normalized Kagan angle of 0.2, or Kagan angle of 24°), to reduce the number of unclassified MT solutions and ensure that only few clusters are found.

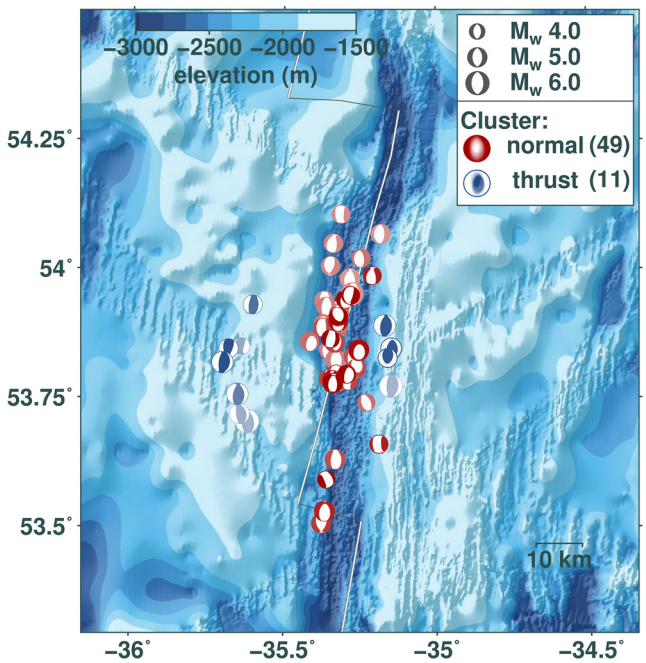

Figure 2. Location of 61 earthquakes after relative relocation and corresponding full moment tensors. Only earthquakes with available clustering are shown. Red and blue color indicate the two moment tensor clusters (overlapping focal spheres for the two clusters are shown in the top right inset), and light to dark color indicate the temporal evolution of seismicity. Only events with successful inversion, relocation, and clustering are shown.

2.3. Centroid Relocation

Relative relocation is important to improve the spatial resolution of seismic sequences. We used the GrowClust3D.jl relocation method (Trugman et al., 2017, 2023), which implements a cluster based relocation scheme based on relative time shifts between arrival times of events with similar waveforms and similar mechanisms. Relative time-shifts are obtained from a moving cross-correlation between vertical signals of two events recorded at the same station filtered in the frequency band 0.015–0.040 Hz. Sixteen events were not relocated due to their remote location off the ridge axis. Also low-quality time shift measurements caused by low SNRs of the waveforms prevented from their relocation. Lag times corresponding to the highest CC value and event-to-station azimuths for several stations are then used to fit a sinusoidal curve. The offset time of the curve is subtracted from the lag times and yields relative measurements. The method requires a high waveform similarity among the different events and clustered initial locations. Time shifts are converted into distance and azimuths using pre-calculated travel times based on a 1D velocity model; the required ray tracing was performed using a ground model with oceanic crust (Cesca et al., 2021). We preprocessed the data to improve accuracy and reliability of the waveform clustering based relocation, such as flipping the signals of the few thrust events due to the high anticorrelation between most signals (Figure S9 in Supporting Information S1). We relocated 61 events of the original catalog using a set of 151,528 time shift measurements with associated normalized CC coefficients larger than 0.75 (Figure S10 in Supporting Information S1). The measurements were derived from broadband stations with epicentral distances smaller than 2,500 km.

2.4. Hypocentral Depth Estimation From Teleseismic Depth Phases

We model the hypocentral depth of the largest three earthquakes (Mw 5.7, 5.8, and 6.0) of the swarm based on the delay of depth phases, pP and sP, at teleseismic distances, using the Abedeto tool (https://github.com/HerrMuellerluedenscheid/abedeto). Synthetic seismograms account for the moment tensor retrieved in this study, a global model for wave propagation (AK135, Kennett et al., 1995) and local models at the source and receiver sites (according to the CRUST 2.0 database, Bassin et al., 2000). Observed seismograms are stacked to improve the signal-to-noise (SNR) ratio. The stack is performed separately for each event and for each array. We performed the depth analysis for 6 different arrays (BCA, BMA, GERES, ILAR, IMAR, YKA, Table S1 in Supporting Information S1), except for a single earthquake where signal-to-noise ration was too low at one array, with different azimuths and epicentral distances. Comparing observations and synthetics for different depths allows us to estimate the centroid depth (Figure S11 in Supporting Information S1).

3. Results

We obtain 77 robust MT solutions (Figures S5 and S6 in Supporting Information S1, Data Sets S2 and S3). The large majority (71 solutions) can be clustered into two main families (Figures S7 and S8 in Supporting Information S1, one characterized by NS normal faulting focal mechanisms (60 earthquakes), and one by NS thrust mechanisms (11). Six remnant MTs remain unclassified (Figure S8 in Supporting Information S1). Full MT (Data Set S2) solutions show a clear pattern for non double couple components, with almost all normal faulting events associated with positive isotropic components, and thrust events with negative ones (Figure S7 in Supporting Information S1). Combining earthquake relocation (Data Set S1) and MT inversion shows that, while normal faulting earthquakes align N-S along the ridge axis, over ∼60 km, thrust mechanisms are located ∼20–30 km off the axis, both to the East and West (Figure 2). The average horizontal relocation uncertainty is 1.3 km (Figure S10 in Supporting Information S1).

Source depths are shallow, with centroid depths spreading ∼7 ± 3 km with an average uncertainty of ∼4 km, according to the MT inversion, and a depth estimate of 2.0 and 3.5–4.0 km for the largest normal faulting (Mw 5.7) and thrust earthquakes (Mw 5.8 and 6.0), respectively, according to deep phase modeling for largest earthquakes

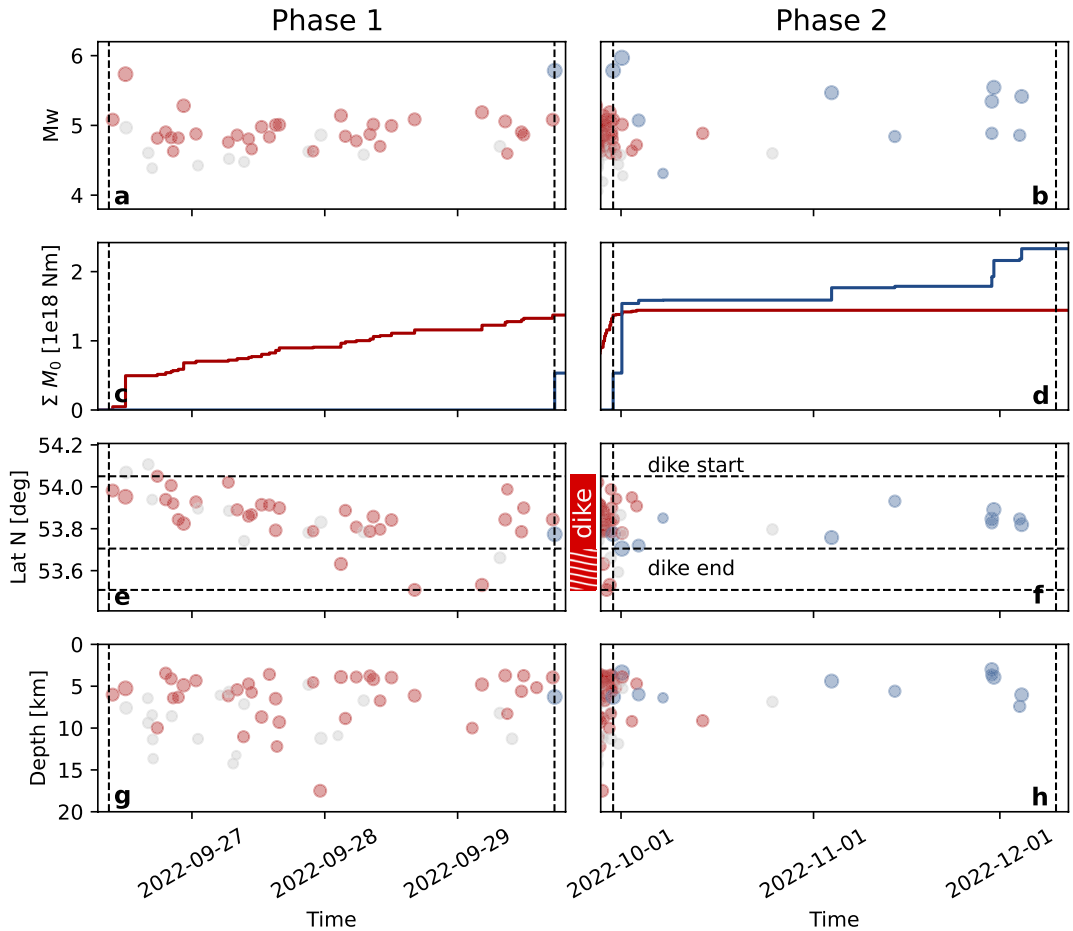

Figure 3. Moment magnitude from moment tensor inversion ((a) Phase 1, time period 26 September 07:00–29 September 2022, 15:30 and (b) Phase 2, time period 29 September 2022, 15:30–10 December 2022, 00:00, dashed vertical lines marking start and end of each phase) and corresponding (c, d) cumulative scalar moment, (e, f) latitude, and (g, h) depth from relocation as a function of time. Dashed horizontal lines in panels (e, f) mark the dike start in the North and potential dike ends in the south, with dike lengths of ~40 and ~60 km. Red color corresponds to normal faulting earthquakes, blue to thrust earthquakes. Earthquakes with unclassified focal mechanisms are in gray. The minimum dike extent and its potential maximal length are marked by solid and striped purple vertical bars, respectively.

(Figure S11 and Table S1 in Supporting Information S1). For each single earthquake, all results for different arrays provide consistent depth estimates. The highest reported magnitude is Mw 6.01 ± 0.05, to date the largest ever reported in the swarm region. Although normal faulting earthquakes are much more abundant, thrust earthquakes are larger. The overall cumulative moment release, M_0, of the swarm is 4.05 10^{18} Nm (equivalent to Mw 6.4), and almost equally released by normal (M_0 = 1.72·10^{18} Nm, Mw 6.1) and thrust ($M0$ = 2.33·10^{18} Nm, Mw 6.2) earthquakes. The temporal evolution of the two families (Figure 3), in change, is different and almost complementary: normal faulting earthquakes are strongly predominant in the first phase, lasting ~3 days from 26 September to 29 September, while thrust mechanisms are absent in the first days (the first thrust event is found on 29 September) and become predominant in the second phase, mostly from October on. As for the spatiotemporal evolution of seismicity, normal faulting earthquakes clearly migrate unilaterally from North to South along axis (Figure 3), over ~60 km (Figure 2), with a small gap at ~53.7°N. The gap roughly corresponds to the latitude of the first thrust earthquakes, while later thrust earthquakes are found slightly northward, with a small lateral migration in the opposite direction (i.e., from South to North).

4. Discussion

Resolving active processes at submarine ridges is difficult. Most of the current knowledge on the mechanics of magmatic rifting has been inferred by rifting observations on land (Ágústsdóttir et al., 2016; Wright et al., 2012). At Krafla, Iceland, for example, during the Krafla volcanic fires episode (1975–1984) ∼20 dikes formed (Buck et al., 2006; Einarsson & Bransdóttir, 1980). The first, and longest dike intrusion, in December 1975, affected a ∼80 km segment of the spreading center, comparable in size with the current observation at the North Atlantic ridge.

Swarm episodes are widespread at MOR, occurring sporadically in time and space. Resolving active processes at submarine ridges is difficult (Wright et al., 2012). MOR swarms typically show moderate magnitudes, well below the detection threshold of global catalogs (Bergman & Solomon, 1990; Schlindwein, 2012). The 2022 swarm at the North Mid-Atlantic Ridge presents different peculiarities. At a local scale, it is outstanding in terms of maximum magnitude and released moment rate (Figure 1). It affected a segment of ∼40–60 km length, which was activated over ∼3 days, starting on September 26, ∼07:00 UTC, involving a similar segment length and comparable duration as the 2010 rifting episode in the western Gulf of Aden (Shuler & Nettles, 2012). Another very unusual aspect concerns the reported focal mechanisms. Thrust mechanisms are rarely reported at MOR (Ruch et al., 2021), where such failure type is incompatible with the dominant extensional stresses. The observation of large off rift thrust earthquakes during the 2022 is quite unique, likely requiring specific conditions. First, the stress perturbation produced by the intrusion needs to be large enough, which seems to be the case for the 2022 intrusion, considering the exceptional triggered seismicity. Next, it also need the presence of pre-existing weaken regions and faults, where thrust faulting can occur. This is valid for cases where parallel rifts and dike intrusions are present.

A main question is whether the swarm had a magmatic or a tectonic origin. Several of the swarm features point at a magmatic origin. A first argument is given by the elongated spatial distribution (Figure 2) of the epicenters (Bergman & Solomon, 1990). Our results show that the seismicity is distributed symmetrically, relative to the ridge axis. This finding offers a second argument for a magmatic driver, as it has been suggested that magmatism-related seismicity is typically centered symmetrically at segment centers, whereas more tectonically driven seismic sequences are located to either side of the rift valley toward segment ends (Escartín et al., 2008; Simao et al., 2010). Other, strong arguments lie in the swarm-like characteristic of the seismic sequence and the spatiotemporal migration of the seismicity (Goslin et al., 2012; Schlindwein, 2012; Simao et al., 2010), and most specifically of normal faulting earthquakes (Shuler & Nettles, 2012), which propagate from North to South (Figure 3). While the northern initiation of the dike at ∼54.1°N is well constrained by the first epicenters, its southern extent may vary between 53.5° and 53.7°N, depending if we consider the entire seismicity or the most dense and thrust earthquakes as a marker for the end of the dike migration. Accordingly, we estimated a dike length of 40–60 km (Figure 3). We estimate an average velocity of ∼0.1–0.3 m/s during Phase 1, which is consistent with migration velocities of seismicity for magma driven swarms in similar tectonic environments: 0.1 m/s at the Bransfield Strait (estimated after Cesca et al., 2022), 0.3 ± 0.1 m/s (Dziak et al., 1995) and not exceeding 0.5 m/s at Krafla (Einarsson & Bransdóttir, 1980). Ágústsdóttir et al. (2016) found migration rates of 0.1–1.3 m/s for the 2014 Bárðarbunga-Holuhraun dike intrusion, Iceland. Finally, a last argument is given by the occurrence of thrust mechanism earthquakes off the ridge axis, mostly in correspondence to a sub-segment with lower normal faulting activity. Analog experiments (Trippanera et al., 2015) showed that thrust mechanisms may be triggered on the side of a magmatic dike, if the dike thickness is large enough and the resulting compressive stress is able to overcome the background tectonic stress.

We hypothesize a scenario able to explain all observed seismicity patterns, sketched in Figure 4, where we identify two distinct phases. In the first phase, a crustal magma intrusion starts at ∼54.1°N, a location marked by the first earthquakes of the swarm; in the ∼EW extensional domain, this leads to the formation of a vertical dike, opening in the EW direction, where the confining stress is smallest, and propagating along the NS direction. The dike propagates unilaterally to the South over ∼3 days. This first phase is accompanied by normal faulting earthquakes above the dike (Cesca et al., 2022; Passarelli et al., 2015). A spatial gap of the normal faulting seismicity at ∼ 53.7°Lat N suggests that the dike migration stops there, and only few sparse earthquakes are observed southward.

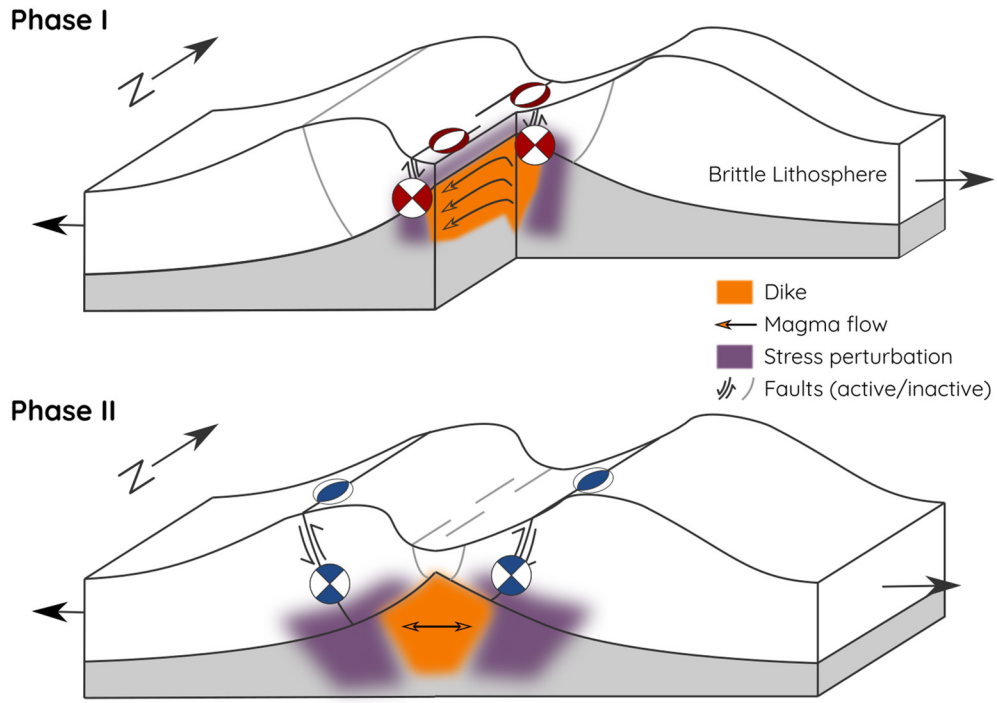

Figure 4. Idealized sketch of the prevailing processes within the different phases recognized by seismicity. Phase I is characterized by shallow magma flow and dike migration along the rift valley from North to South with a stress perturbation near the rift valley causing shallow normal faulting above the dike. In the later phase II the dike stops propagating along the rift valley and thickens instead. This causes a stress state favoring the activation of old faults on the flanks of the ridge with large thrust earthquakes.

The end of the dike propagation marks the beginning of the second phase. A reason for the dike stop could be the presence of a warmer region, eventually a former spreading center, or a structural or geometrical anomaly of the rift valley, where the dike is inhibited to further propagate and can thicken. This hypothesis would also explain why the first thrust mechanisms are observed at this range of latitudes: the increased dike thickness would produce here a stronger stress perturbation, which locally overcomes the background stress and favors the occurrence of thrust mechanisms on pre-existing structures, parallel to the ridge axis. The fact that a few further thrust earthquakes occur later slightly northward could be explained by the combined effect of the stress perturbation introduced by the dike itself and the Coulomb stress transferred by the first thrust earthquakes.

An alternative model for thrust earthquakes could involve the failure of outward dipping faulting on top of a depleting shallow reservoir, similar as observed during the first stage of calderas formation (Acocella, 2007; Levy et al., 2018). There are a few observations which make such a scenario less likely. First, the distance among the thrust earthquakes located West and East of the ridge, which could mark the reservoir sides, is in the order of ~30 km, which would imply an exceptionally large caldera diameter. Next, this model hardly explains the geometry of the seismicity: the dike starts at ~54.1°N, arguably in the vicinity of a feeding reservoir, but this location is inconsistent with the one of thrust earthquakes (~53.8°N), which would mark the forming caldera.

Given our interpretation that normal faulting events occur at shallow depths above a vertical dike, we use empirical relations to link the cumulative moment of triggered normal faulting seismicity to the volume of magma intruded (White & McCausland, 2016); this relation was derived based on a broad data set of volcano-tectonic earthquakes preceding eruptions and may only provide a first order estimate. We estimate a magma volume of ~0.53 km^3, which is comparable to recent intrusion at the rifting-to-spreading Bransfield Strait Basin (Cesca et al., 2022). However, the moment is released differently by the two earthquake families: the thrust family counts 11 earthquakes only, but has relatively high magnitudes, given the intruded magma volume.

5. Conclusions

This study targets a large swarm at a remote location along the North Atlantic Mid-Ocean Ridge. Beside the remoteness of the study region and the lack of local seafloor installation, we could reconstruct the evolution of seismicity by the analysis of regional, teleseismic and array data and the application of waveform based techniques. The analysis has also been possible thanks to the outstanding large involved magnitudes, reaching Mw 6.0, as the seismic swarm substantially exceeded previous seismicity in the focal region both in terms of rates and moment release. Beside the unusual size of the seismicity, another intriguing feature of the 2022 swarm is the presence of thrust mechanisms, which are unusual at a mid-ocean ridge. While in the first phase normal faulting earthquakes are predominant, in the second phase, from the end of September onward, thrust mechanisms appear and become more frequent. Indeed, largest magnitude earthquakes occurred with a thrust mechanism and off the ridge axes.

Unilateral migration, elongated spatial pattern of the epicenters and presence of both normal and thrust focal mechanisms suggest a magmatic driven swarm. Our model to explain the seismological observations includes two phases. In the first one, starting on 26 September 2022, at ∼07:00 UTC, the dike intrudes and propagates unilaterally southward ∼60 km, triggering shallow normal faulting earthquakes above the intrusion. We hypothesize that, in the second phase the dike stops and thickens at its Southern segment. Seismicity accompanying the second phase is mostly characterized by off-ridge thrust earthquakes, which are triggered by a compressive stress transient induced by the thicker dike. We estimated the volume of the magmatic intrusion as ∼0.53 km^3. The 2022 unrest provides evidence for sporadic spreading accompanied by large swarm episodes and earthquakes with both normal and thrust faulting focal mechanisms controlled by magma intrusions at the Mid-Atlantic Ridge.

Data Availability Statement

All seismic data used in this study (Figure S1 in Supporting Information S1 shows the distribution of seismic stations and arrays used) are open and accessible via the Incorporated Research Institutions for Seismology (IRIS) Data Management Center (https://service.iris.edu/), GEOFON (GEO-ForschungsNetz) (https://geofon.gfz-potsdam.de/waveform/webservices/), ORFEUS EIDA (Observatories and Research Facilities for European Seismology - European Integrated Data Archive) (http://www.orfeus-eu.org/data/eida/webservices), and NORSAR (the Norwegian National Data Center) (https://www.norsar.no). We used broadband data from the seismic networks C8 (Canadian Seismic Research Network), CN (Canadian National Seismograph Network) (Natural Resources Canada, 1975), DK (Danish Seismological Network), EI (Irish National Seismic Network, INSN) (Dublin Institute for Advanced Studies, 1993), G (French Global Network of Seismological Broadband Stations, GEOSCOPE) (Institut de physique du globe de Paris (IPGP) and École et Observatoire des Sciences de la Terre de Strasbourg (EOST), 1982), GB (Great Britain Seismograph Network), GE (GEOFON) (GEOFON Data Centre, 1993), II (Global Seismograph Network - IRIS/IDA, GSN) (Scripps Institution of Oceanography, 1986), IU (Global Seismograph Network (GSN - IRIS/USGS), GSN) (Albuquerque Seismological Laboratory/USGS, 2014), PM (Portuguese National Seismic Network) (Instituto Português do Mar e da Atmosfera, I.P., 2006), and array data from BCA (Beaver Creek Array, Alaska, USA), BMA (Burnt Mountain Array, Alaska, USA), GERES (GERESS Array Beam, Bayern, Germany), ILAR (ILAR Array Beam, Eilson, AK, USA), IMAR (Indian Mountain Array, Alaska, USA), NOA (NORSAR) (Norsar, 1971), YKA (Yellowknife Array Beam, Canada). Bathymetry was downloaded from GMRT (Ryan et al., 2009). A list of networks used, and their references are listed in Supporting Information S1. Software used is open source, and either available at the repositories cited in the manuscript or available upon request to the authors. Data Sets S1, S2, and S3 are openly available (https://doi.org/10.5281/zenodo.8089070).

Acknowledgments
We are thankful to the editor, Prof. Dr. G. Prieto, Prof. Dr. V. Schlindwein, and an anonymous reviewer for a careful review and constructive suggestions. M.M. was supported by the BMBF project EWRICA (03G0891B). P.B. has also received funding by the Deutsche Forschungsgemeinschaft (DFG, German Research Foundation) Project 407141557. All seismic data used in this study are open (see Data Availability) and a list of networks used and their references are listed in Supporting Information S1. Open Access funding enabled and organized by Projekt DEAL.

References

Acocella, V. (2007). Understanding caldera structure and development: An overview of analogue models compared to natural calderas. *Earth-Science Reviews*, *85*(3–4), 125–160. https://doi.org/10.1016/j.earscirev.2007.08.004

Ágústsdóttir, T., Winder, T., Woods, J., White, R. S., Greenfield, T., & Brandsdóttir, B. (2019). Intense seismicity during the 2014–2015 Bárðarbunga-Holuhraun rifting event, Iceland, reveals the nature of dike-induced earthquakes and caldera collapse mechanisms. *Journal of Geophysical Research: Solid Earth*, *124*(8), 8331–8357. https://doi.org/10.1029/2018jb016010

Ágústsdóttir, T., Woods, J., Greenfield, T., Green, R. G., White, R. S., Winder, T., et al. (2016). Strike-slip faulting during the 2014 Bárðarbunga-Holuhraun dike intrusion, central Iceland. *Geophysical Research Letters*, *43*(4), 1495–1503. https://doi.org/10.1002/2015gl067423

Albuquerque Seismological Laboratory/USGS. (2014). Global seismograph network (GSN - IRIS/USGS) [Dataset]. International Federation of Digital Seismograph Networks. https://doi.org/10.7914/SN/IU

Bassin, C., Laske, G., & Masters, G. (2000). The current limits of resolution for surface wave tomography in North America. *EOS Trans. AGU*, *81*, F897.

Benoit, J. P., & McNutt, S. R. (1996). Global volcanic earthquake swarm database and preliminary analysis of volcanic earthquake swarm duration. *Annali di Geofisica*, *39*(2), 221.

Bergman, E. A., & Solomon, S. (1990). Earthquake swarms on the Mid-Atlantic Ridge - Products of magmatism or extensional tectonics? *Journal of Geophysical Research*, *95*(B4), 4943–4965. https://doi.org/10.1029/JB095iB04p04943

Bird, P. (2003). An updated digital model of plate boundaries. *Geochemistry, Geophysics, Geosystems*, *4*(3), 1027. https://doi.org/10.1029/2001GC000252

Buck, W. R., Einarsson, P., & Brandsdóttir, B. (2006). Tectonic stress and magma chamber size as controls on dike propagation: Constraints from the 1975–1984 Krafla rifting episode. *Journal of Geophysical Research*, *111*(B12), B12404. https://doi.org/10.1029/2005jb003879

Bungum, H., Husebye, E. S., & Ringdal, F. (1971). The NORSAR array and preliminary results of data analysis. *Geophysical Journal of the Royal Astronomical Society*, *25*(1–3), 115–126. https://doi.org/10.1111/j.1365-246x.1971.tb02334.x

Cesca, S. (2020). Seiscloud, a tool for density-based seismicity clustering and visualization. *Journal of Seismology*, *24*(3), 443–457. https://doi.org/10.1007/s10950-020-09921-8

Cesca, S., Letort, J., Razafindrakoto, H. N. T., Heimann, S., Rivalta, E., Isken, M. P., et al. (2020). Drainage of a deep magma reservoir near Mayotte inferred from seismicity and deformation. *Nature Geoscience*, *13*(1), 87–93. https://doi.org/10.1038/s41561-019-0505-5

Cesca, S., Sugan, M., Rudzinski, Ł., Vajedian, S., Niemz, P., Plank, S., et al. (2022). Massive earthquake swarm driven by magmatic intrusion at the Bransfield Strait, Antarctica. *Communications Earth & Environment*, *3*(1), 1–11. https://doi.org/10.1038/s43247-022-00418-5

Cesca, S., Valenzuela Malebrán, C., López-Comino, J. Á., Davis, T., Tassara, C., Oncken, O., & Dahm, T. (2021). The 2014 Juan Fernández microplate earthquake doublet: Evidence for large thrust faulting driven by microplate rotation. *Tectonophysics*, *801*, 228720. https://doi.org/10.1016/j.tecto.2021.228720

Chen, X., & Shearer, P. M. (2011). Comprehensive analysis of earthquake source spectra and swarms in the Salton Trough, California. *Journal of Geophysical Research*, *116*(B9), B09309. https://doi.org/10.1029/2011jb008263

Dublin Institute for Advanced Studies. (1993). Irish National seismic network [Dataset]. International Federation of Digital Seismograph Networks. https://doi.org/10.7914/SN/EI

Dziak, R. P., Bohnenstiehl, D., Cowen, J., Baker, E., Rubin, K., Haxel, J., & Fowler, M. (2007). Rapid dike emplacement leads to eruptions and hydrothermal plume release during seafloor spreading events. *Geology*, *35*(7), 579–582. https://doi.org/10.1130/g23476a.1

Dziak, R. P., Bohnenstiehl, D. R., Matsumoto, H., Fowler, M. J., Haxel, J. H., Tolstoy, M., & Waldhauser, F. (2006). January 2006 seafloor-spreading event at 9 50′N, East Pacific Rise: Ridge dike intrusion and transform fault interactions from regional hydroacoustic data. *Geochemistry, Geophysics, Geosystems*, *10*(6), Q06T06. https://doi.org/10.1029/2009gc002388

Dziak, R. P., Fox, C. G., & Schreiner, A. E. (1995). The June-July 1993 seismo-acoustic event at CoAxial segment, Juan de Fuca Ridge: Evidence for a lateral dike injection. *Geophysical Research Letters*, *22*(2), 135–138. https://doi.org/10.1029/94gl01857

Dziak, R. P., Haxel, J. H., Bohnenstiehl, D. R., Chadwick, W. W., Nooner, S. L., Fowler, M. J., et al. (2012). Seismic precursors and magma ascent before the April 2011 eruption at Axial Seamount. *Nature Geoscience*, *5*(7), 478–482. https://doi.org/10.1038/ngeo1490

Einarsson, P., & Bransdóttir, B. (1980). Seismological evidence for lateral magma intrusion during the July 1978 deflation of the Krafla volcano in NE-Iceland. *Journal of Geophysics*, *47*, 160–165.

Escartín, J., Smith, D. K., Cann, J., Schouten, H., Langmuir, C. H., & Escrig, S. (2008). Central role of detachment faults in accretion of slow-spreading oceanic lithosphere. *Nature*, *455*(7214), 790–794. https://doi.org/10.1038/nature07333

Ester, M., Kriegel, H. P., Sander, J., & Xu, X. (1996). A density-based algorithm for discovering clusters in large spatial databases with noise. In E. Simoudis, J. Han, & U. M. Fayyad (Eds.), *Proceedings of the second international conference on knowledge discovery and data mining* (pp. 226–231). AAAI Press.

GEOFON Data Centre. (1993). GEOFON seismic network. *Deutsches GeoForschungsZentrum GFZ*. https://doi.org/10.14470/TR560404

Gibbons, S. J., & Ringdal, F. (2006). The detection of low magnitude seismic events using array-based waveform correlation. *Geophysical Journal International*, *165*(1), 149–166. https://doi.org/10.1111/j.1365-246X.2006.02865.x

Giusti, M., Perrot, J., Dziak, R. P., Sukhovich, A., & Maia, M. (2018). The August 2010 earthquake swarm at north FAMOUS–FAMOUS segments, Mid-Atlantic Ridge: Geophysical evidence of dike intrusion. *Geophysical Journal International*, *215*(1), 181–195. https://doi.org/10.1093/gji/ggy239

Goslin, J., Perrot, J., Royer, J. Y., Martin, C., Lourenço, N., Luis, J., et al. (2012). Spatiotemporal distribution of the seismicity along the Mid-Atlantic Ridge north of the Azores from hydroacoustic data: Insights into seismogenic processes in a ridge–hot spot context. *Geochemistry, Geophysics, Geosystems*, *13*(2), Q02010. https://doi.org/10.1029/2011gc003828

Heimann, S., Isken, M., Kühn, D., Sudhaus, H., Steinberg, A., Daout, S., et al. (2018). *Grond - A probabilistic earthquake source inversion framework. V. 1.0*. GFZ Data Services. https://doi.org/10.5880/GFZ.2.1.2018.003

Hill, D. P. (1977). A model for earthquake swarms. *Journal of Geophysical Research*, *82*(8), 1347–1352. https://doi.org/10.1029/jb082i008p01347

Institut de physique du globe de Paris (IPGP) and École et Observatoire des Sciences de la Terre de Strasbourg (EOST). (1982). *GEOSCOPE, French Global Network of broad band seismic stations*. Institut de physique du globe de Paris (IPGP), Université de Paris. https://doi.org/10.18715/GEOSCOPE.G

Instituto Português do Mar e da Atmosfera, I.P. (2006). Portuguese national seismic network [Dataset]. International Federation of Digital Seismograph Networks. https://doi.org/10.7914/SN/PM

International Seismological Centre. (2022). On-line Bulletin. https://doi.org/10.31905/D808B830

Isacks, B., Oliver, J., & Sykes, L. R. (1968). Seismology and the new global tectonics. *Journal of Geophysical Research*, *73*(18), 5855–5899. https://doi.org/10.1029/jb073i018p05855

Kagan, Y. Y. (1991). 3-D rotation of double-couple earthquake sources. *Geophysical Journal International*, *106*(3), 709–716. https://doi.org/10.1111/j.1365-246x.1991.tb06343.x

Kagan, Y. Y. (1992). Correlation of earthquake focal mechanisms. *Geophysical Journal International*, *110*(2), 305–320. https://doi.org/10.1111/j.1365-246x.1992.tb00876.x

Keir, D., Hamling, I. J., Ayele, A., Calais, E., Ebinger, C., Wright, T. J., et al. (2009). Evidence for focused magmatic accretion at segment centers from lateral dike injections captured beneath the Red Sea rift in Afar. *Geology*, *37*(1), 59–62. https://doi.org/10.1130/g25147a.1

Kennett, B. L. N., Engdahl, E. R., & Buland, R. (1995). Constraints on seismic velocities in the Earth from travel times. *Geophysical Journal International*, *122*(1), 108–124. https://doi.org/10.1111/j.1365-246X.1995.tb03540.x

Le Pichon, X. (1968). Sea-floor spreading and continental drift. *Journal of Geophysical Research*, *73*(3), 3661–3697. https://doi.org/10.1029/jb073i012p03661

Levy, S., Bohnenstiehl, D., Sprinkle, P., Boettcher, M., Wilcock, W., Tolstoy, M., & Waldhauser, F. (2018). Mechanics of fault reactivation before, during, and after the 2015 eruption of axial seamount. *Geology*, *46*(5), 447–450. https://doi.org/10.1130/g39978.1

Llenos, A. L., & van der Elst, N. J. (2019). Improving earthquake forecasts during swarms with a duration ModelImproving earthquake forecasts during swarms with a duration model. *Bulletin of the Seismological Society of America*, *109*(3), 1148–1155. https://doi.org/10.1785/0120180332

Meier, M., Schlindwein, V., Scholz, J., Geils, J., Schmidt-Aursch, M. C., Krüger, F., et al. (2021). Segment-scale seismicity of the ultraslow spreading Knipovich Ridge. *Geochemistry, Geophysics, Geosystems*, *22*(2), e2020GC009375. https://doi.org/10.1029/2020gc009375

Müller, C., & Jokat, W. (2000). Seismic evidence for volcanic activity discovered in central Arctic. *Eos, Transactions American Geophysical Union*, *81*(24), 265–269. https://doi.org/10.1029/00eo00186

Müller, R. D., Sdrolias, M., Gaina, C., & Roest, W. R. (2008). Age, spreading rates, and spreading asymmetry of the world's ocean crust. *Geochemistry, Geophysics, Geosystems*, *9*(4), Q04006. https://doi.org/10.1029/2007gc001743

Natural Resources Canada (NRCAN Canada). (1975). Canadian national seismograph network [Dataset]. International Federation of Digital Seismograph Networks. https://doi.org/10.7914/SN/CN

Norsar. (1971). NORSAR station network [Dataset]. NORSAR. https://doi.org/10.21348/d.no.0001

Parnell-Turner, R., Sohn, R. A., Peirce, C., Reston, T. J., MacLeod, C. J., Searle, R. C., & Simão, N. M. (2017). Oceanic detachment faults generate compression in extension. *Geology*, *45*(10), 923–926. https://doi.org/10.1130/g39232.1

Passarelli, L., Heryandoko, N., Cesca, S., Rivalta, E., Rasmid, Rohadi, S., et al. (2018). Magmatic or not magmatic? The 2015–2016 seismic swarm at the long-dormant Jailolo volcano, West Halmahera, Indonesia. *Frontiers in Earth Science*, *6*, 79. https://doi.org/10.3389/feart.2018.00079

Passarelli, L., Rivalta, E., Cesca, S., & Aoki, Y. (2015). Stress changes, focal mechanisms, and earthquake scaling laws for the 2000 dike at Miyakejima (Japan). *Journal of Geophysical Research: Solid Earth*, *120*(6), 4130–4145. https://doi.org/10.1002/2014jb011504

Passarelli, L., Rivalta, E., Jónsson, S., Hensch, M., Metzger, S., Jakobsdóttir, S. S., et al. (2018). Scaling and spatial complementarity of tectonic earthquake swarms. *Earth and Planetary Science Letters*, *482*, 62–70. https://doi.org/10.1016/j.epsl.2017.10.052

Peng, Z., & Zhao, P. (2009). Migration of early aftershocks following the 2004 Parkfield earthquake. *Nature Geoscience*, *2*(12), 877–881. https://doi.org/10.1038/ngeo697

Radha Krishna, M., & Arora, S. K. (1998). Space-time seismicity and earthquake swarms: Certain observations along the slow-spreading mid-Indian Ocean ridges. *Proceedings of the Indian Academy of Sciences - Section A*, *107*(2), 161–17. https://doi.org/10.1007/bf02840467

Rivalta, E., Taisne, B., Bunger, A. P., & Katz, R. F. (2015). A review of mechanical models of dike propagation: Schools of thought, results and future directions. *Tectonophysics*, *638*, 1–42. https://doi.org/10.1016/j.tecto.2014.10.003

Roland, E., & McGuire, J. J. (2009). Earthquake swarms on transform faults. *Geophysical Journal International*, *178*(3), 1677–1690. https://doi.org/10.1111/j.1365-246x.2009.04214.x

Ruch, J., Keir, D., Passarelli, L., Di Giacomo, D., Ogubazghi, G., & Jónsson, S. (2021). Revealing 60 years of earthquake swarms in the southern Red Sea, Afar and the Gulf of Aden. *Frontiers in Earth Science*, *9*, 664673. https://doi.org/10.3389/feart.2021.664673

Rundquist, D. V., & Sobolev, P. O. (2002). Seismicity of mid-oceanic ridges and its geodynamic implications: A review. *Earth-Science Reviews*, *58*(1–2), 143–161. https://doi.org/10.1016/S0012-8252(01)00086-1

Ryan, W. B. F., Carbotte, S. M., Coplan, J. O., O'Hara, S., Melkonian, A., Arko, R., et al. (2009). Global multi-resolution topography synthesis. *Geochemistry, Geophysics, Geosystems*, *10*(3), Q03014. https://doi.org/10.1029/2008GC002332

Schlindwein, V. (2012). Teleseismic earthquake swarms at ultraslow spreading ridges: Indicator for dyke intrusions? *Geophysical Journal International*, *190*(1), 442–456. https://doi.org/10.1111/j.1365-246X.2012.05502.x

Scripps Institution of Oceanography. (1986). Global seismograph network - IRIS/IDA [Dataset]. International Federation of Digital Seismograph Networks. https://doi.org/10.7914/SN/II

Searle, R. (2013). *Mid-ocean ridges*. Cambridge University Press.

Shuler, A., & Nettles, M. (2012). Earthquake source parameters for the 2010 western Gulf of Aden rifting episode. *Geophysical Journal International*, *190*(2), 1111–1122. https://doi.org/10.1111/j.1365-246X.2012.05529.x

Sigmundsson, F., Hooper, A., Hreinsdóttir, S., Vogfjörd, K. S., Ófeigsson, B. G., Heimisson, E. R., et al. (2015). Segnented lateral dyke growth in a rifting event at Bárðarbunga volcanic system, Iceland. *Nature*, *517*(7533), 191–195. https://doi.org/10.1038/nature14111

Sigmundsson, F., Parks, M., Hooper, A., Geirsson, H., Vogfjörd, K. S., Drouin, V., et al. (2022). Deformation and seismicity decline before the 2021 Fagradalsfjall eruption. *Nature*, *609*(7927), 523–528. https://doi.org/10.1038/s41586-022-05083-4

Simao, N., Escartin, J., Goslin, J., Haxel, J., Cannat, M., & Dziak, R. (2010). Regional seismicity of the Mid-Atlantic Ridge: Observations from autonomous hydrophone arrays. *Geophysical Journal International*, *183*(3), 1559–1578. https://doi.org/10.1111/j.1365-246x.2010.04815.x

Sykes, L. R. (1967). Mechanism of earthquakes and nature of faulting on the mid-oceanic ridges. *Journal of Geophysical Research*, *72*(8), 2131–2153. https://doi.org/10.1029/jz072i008p02131

Sykes, L. R. (1970). Earthquake swarms and sea-floor spreading. *Journal of Geophysical Research*, *75*(32), 6598–6611. https://doi.org/10.1029/jb075i032p06598

Tolstoy, M., Bohnenstiehl, D. R., Edwards, M. H., & Kurras, G. J. (2001). Seismic character of volcanic activity at the ultraslow-spreading Gakkel Ridge. *Geology*, *29*(12), 1139–1142. https://doi.org/10.1130/0091-7613(2001)029<1139:scovaa>2.0.co;2

Trippanera, D., Ruch, J., Acocella, V., & Rivalta, E. (2015). Experiments of dike-induced deformation: Insights on the long-term evolution of divergent plate boundaries. *Journal of Geophysical Research: Solid Earth*, *120*(10), 6913–6942. https://doi.org/10.1002/2014jb011850

Trugman, D. T., Chamberlain, C. J., Savvaidis, A., & Lomax, A. (2023). GrowClust3D.jl: A Julia package for the relative relocation of earthquake hypocenters using 3D velocity models. *Seismological Research Letters*, *94*(1), 443–456. https://doi.org/10.1785/0220220193

Trugman, D. T., Dougherty, S. L., Cochran, E. S., & Shearer, P. M. (2017). Source spectral properties of small to moderate earthquakes in southern Kansas. *Journal of Geophysical Research: Solid Earth*, *122*(10), 8021–8034. https://doi.org/10.1002/2017JB014649

Wauthier, C., Stephens, K., Oliva, S. J., Weinstein, A., & Ebinger, C. J. (2016). Magmatic fluid processes revealed by a joint analysis of seismic and InSAR data in an early continental rift. In *AGU Fall Meeting Abstracts*, (Vol. 2016, p. T51C-2928).

Weidner, D. J., & Aki, K. (1973). Focal depth and mechanism of mid-ocean ridge earthquakes. *Journal of Geophysical Research*, *78*(11), 1818–1831. https://doi.org/10.1029/jb078i011p01818

White, R., & McCausland, W. (2016). Volcano-tectonic earthquakes: A new tool for estimating intrusive volumes and forecasting eruptions. *Journal of Volcanology and Geothermal Research*, *309*, 139–155. https://doi.org/10.1016/j.jvolgeores.2015.10.020

Wolfe, C. J., Bergman, E. A., & Solomon, S. C. (2012). Oceanic transform earthquakes with unusual mechanisms or locations: Relation to fault geometry and state of stress in the adjacent lithosphere. *Journal of Geophysical Research*, *98*(B9), 16187–16211. https://doi.org/10.1029/93JB00887

Wright, T. J., Sigmundsson, F., Pagli, C., Belachew, M., Hamling, I. J., Brandsdóttir, B., et al. (2012). Geophysical constraints on the dynamics of spreading centres from rifting episodes on land. *Nature Geoscience*, *5*(4), 242–250. https://doi.org/10.1038/NGEO1428